

**N₂O₅ Hydrolysis on Sub-Micron Organic Aerosols: The Effect of
Relative Humidity, Particle Phase, and Particle Size**

Joel A. Thornton*, Christine F. Braban, Jonathan P. D. Abbatt

Department of Chemistry, University of Toronto, Toronto, ON, Canada

short title: N₂O₅ Hydrolysis on Organic Aerosols

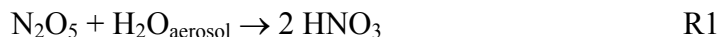
Submitted to *Physical Chemistry and Chemical Physics* June 30, 2003

*Correspondence: Joel Thornton
Dept. of Chemistry, University of Toronto
80 St. George St.
Toronto, ON M5S 3H6 Canada
Tel/Fax: 416-946-7359; jthornto@chem.utoronto.ca

Abstract Measurements of the reactive uptake coefficient for N₂O₅ hydrolysis, γ_m , on sub-micron organic aerosols were performed in an entrained aerosol flow tube as a function of relative humidity (RH), aerosol phase, N₂O₅ partial pressure, and mean aerosol size. Aerosol phase and relative humidity were determined simultaneously, and chemical ionization mass spectrometry was used to detect the decay rate of N₂O₅ in the presence of malonic acid or azelaic acid aerosol. The γ_m on solid malonic acid was determined to be less than 0.001 (RH = 10 – 50%), and on solid azelaic acid, γ_m was 0.0005 ± 0.0003 . Aqueous malonic acid aerosol yielded $\gamma_m = 0.0020 \pm 0.0005$ at 10% RH and increased with RH to ~ 0.03 at RH = 50 – 70%. We report the first evidence of an inverse dependence of the γ_m on the initial partial pressure of N₂O₅ in the flow reactor, and a dependence on particle size for aerosol with surface area-weighted radii less than ~ 100 nm at 50% RH. We find that the super-saturated malonic acid aerosol results are consistent with N₂O₅ hydrolysis being both aerosol volume-limited where, for RH < 50%, water is the limiting reagent, and also with a surface-specific process.

1. Introduction

The heterogeneous hydrolysis of N₂O₅, via reaction R1,



to yield HNO₃ on atmospheric aerosol is now known to play a crucial role in regulating O₃ destruction in the stratosphere,¹ and is expected to play an important role in regulating the oxidative capacity of the troposphere.² Its importance is due to the fact that R1 is a net sink of atmospheric nitrogen oxide radicals (NO_x ≡ NO + NO₂ + NO₃). For example, theoretical studies suggest that incorporation of reaction R1 into global tropospheric chemistry models with a reactive uptake coefficient (i.e. the probability of reaction given a collision with the surface) of $\gamma = 0.1$, leads to a 50% reduction of the winter-time NO_x budget in the mid-latitude northern hemisphere^{2,3} and reductions of order 10-20% in O₃ and OH,² the dominant tropospheric oxidants. Recent *in situ* measurements confirm the importance of N₂O₅ as a nighttime NO_x reservoir in the planetary boundary layer,⁴ and modeling studies constrained by measurements of NO_x provide indirect support for the importance of R1 in the rural and remote troposphere.^{5,6}

A primary motivation for the work presented here is that there are few, if any, determinations of the rate of R1 on organic aerosols over a large range of relative humidity. Organic aerosols are ubiquitous throughout the troposphere and their composition can range from mainly hygroscopic material to hydrophobic.⁷ Recent *in situ* aerosol mass spectrometry measurements have shown that organic matter is almost always associated with tropospheric aerosol,⁸ and it can be the dominant fraction by mass (> 90%) in polluted regions near anthropogenic combustion and biomass burning sources.⁹ A second motivation is that laboratory studies have shown that aerosols, both

organic^{10,11} and inorganic,¹² can undergo phase transitions forming solid and aqueous solutions. Depending on the relative humidity (RH), aqueous aerosols can range from super-saturated to dilute solutions. *In situ* hygroscopic growth measurements corroborate these studies showing atmospheric aerosol taking up and losing water when exposed to higher or lower RH, respectively.¹³ The impact of varying water concentration via relative humidity and aerosol phase changes on the uptake coefficient for R1 is still poorly understood. Studies have demonstrated that reaction R1 proceeds at least an order of magnitude more slowly on dry, solid particles than on aqueous solutions of the same aerosol substrate.¹⁴⁻¹⁸ However, there has been only one study to clearly control and monitor the phase and water content of sulfate aerosol during an experimental determination,¹⁸ and none to our knowledge for organic aerosols.

We report uptake coefficients for N₂O₅ hydrolysis on two organic aerosol substrates, malonic acid (HOOCCH₂COOH) and azaleic acid (HOOC(CH₂)₇COOH). Both compounds are organic diacids, which are often large fractions of identified organic components of atmospheric aerosol.¹⁹ Pure malonic acid aerosol exhibit phase transitions between solid and aqueous particles the latter being super-saturated solutions for RH 10-70% (at room temperature).¹⁰ Azaleic acid, however, is expected to remain a solid particle for RH less than ~ 100%. These two model aerosol systems therefore provide the ability to test the reactivity of N₂O₅ on both hydrophobic and hygroscopic aerosol particles over a wide range of RH and liquid water content. Our approach is unique in that we use an entrained aerosol flow tube coupled to a chemical ionization mass spectrometer to monitor the decay rate of N₂O₅ in the presence of these aerosol particles, and we simultaneously characterize the aerosol phase and RH by using FT-IR aerosol

flow-tube spectroscopy. We present results as a function of RH, aerosol liquid water content, and mean aerosol size.

2. Experimental

2.1 Aerosol Generation and Characterization

Figure 1 shows a schematic of the experimental setup used to generate and characterize solid and aqueous malonic acid aerosol. A constant output atomizer (TSI 3076) was used to generate polydisperse distributions of malonic acid aerosol from 0.1 – 10 wt% aqueous solutions. To create solid malonic acid aerosol, a small fraction (~ 1/5) of the atomizer output was directed through a variable length diffusion dryer (TSI 3062) containing silica gel which dropped the RH below 5%. Previous work in this lab has shown that this RH is sufficiently low to effloresce malonic acid aerosol.¹⁰ After passing through the dryer, the aerosol flow was mixed with a humidified N₂ flow of ~ 3-4 slpm. For the study of aqueous malonic acid particles, the small fraction of the atomizer output was mixed directly with the humidified bulk N₂ flow bypassing the diffusion dryer.

To determine particle phase, the humidified aerosol flow was allowed to equilibrate in a vertically oriented 3 cm ID pyrex flow tube 50 cm long (~ 20 s) where the aerosol adjusts their composition to the surrounding RH, and then passed directly into another flow tube (3 cm ID, 1 m long) oriented perpendicular to the equilibration region. An infrared beam from a Fourier Transform Infrared (FTIR) spectrometer (ABB Bomem MB series) passed axially down the length of this latter tube to an MCT detector. The RH and aerosol phase were determined simultaneously using gas-phase H₂O and both condensed-phase H₂O and malonic acid absorption features, respectively. The RH of the

bulk flow was controlled by mixing different proportions of a dry N₂ flow with a flow of N₂ passed through a water bubbler. The RH determination using gas phase H₂O absorption features is accurate to about $\pm 2\%$.¹⁰ Some of the experiments bypassed the FTIR flow tube when phase characterization was not necessary. For these experiments, the same fraction of atomizer output was mixed with the humidified bulk N₂ flow and transported through approximately 3 m of 1.27 cm OD Teflon tubing (residence time ~ 10 s). A commercial hygrometer probe (VWR) inserted into the humidified aerosol flow at the end of this length of tubing was used to determine the RH. The hygrometer has a stated accuracy of $\pm 2\%$ and typically agreed with the independently calibrated FT-IR approach to within this margin. Over the course of an experiment, the RH of the aerosol flow was constant to within $\sim 1\%$.

For a detailed discussion of the phase transitions of malonic acid aerosol as a function of temperature and RH see *Braban et al.*¹⁰ Briefly, solid malonic acid aerosol deliquesce to become saturated aqueous solutions at 69% RH and room temperature. At the deliquescence RH, the aerosol composition, in mass fraction, is approximately 0.65 malonic acid and 0.45 liquid water.^{10,11} Until the deliquescence point is reached, very little water uptake by solid malonic acid aerosol is observed.^{10,11} At relative humidities greater than this point, the aerosol particles spontaneously take on water, growing and becoming more dilute with respect to malonic acid. As the RH surrounding aqueous malonic acid aerosol is lowered below the deliquescence point, water evaporates from the particles but the aerosol remains as super-saturated solutions down to RH $< 10\%$ due to a free energy barrier to crystal formation. For example, at 50% RH the malonic acid mass

fraction (χ_{MA}) is estimated to be 0.8, while at 10% RH $\chi_{\text{MA}} \sim 0.98$. Malonic acid aerosol effloresce below 7% RH.¹⁰

After passing through the phase characterization region, the aerosol flow passed through a 3 m length of 1.3 cm OD Teflon tubing to the top of the vertically oriented aerosol kinetics flow reactor. At this point a small fraction of aerosol flow ($\sim 0.35 - 0.45$ slpm) was drawn to the scanning mobility particle sizing (SMPS) instrument consisting of a Differential Mobility Analyzer (DMA, TSI 3080-3081) for size selection followed by a condensation particle counter (CPC). A scan over the mobility diameter range of 20 nm – 1000 nm produced a size-distribution from which total aerosol surface area concentration was determined.

Figure 2 shows plots of typical number (top panel) and surface area (bottom panel) size distributions obtained during experiments where 0.1, 0.3, and 1.0 wt% malonic acid solutions were used in the atomizer and subjected to a final RH of 50%. Because the final aerosol composition is controlled by the water activity (i.e., RH), atomizing a more concentrated solution requires larger uptake of water to attain the equilibrium aerosol composition and thus leads to larger mean particle sizes. The number weighted geometric mean diameters, d_{gm} , for the 0.1, 0.3, and 1.0 wt% malonic acid solutions are 56, 63, and 75 nm, respectively, all with geometric standard deviations, σ_{g} , of 2.14. This method was used to study the dependence of N₂O₅ reaction probabilities on aerosol size. Surface area weighted geometric mean diameters for aerosol populations generated from the 0.1, 0.3, and 1 wt% malonic acid solutions are 192, 213, 286 nm, respectively, all with $\sigma_{\text{g}} \sim 2.05$ (see Figure 2). The same atomizing solution was used during an entire experiment so that the distribution characteristics remained constant. To

change the total aerosol surface area during an experiment, the aerosol number density was adjusted by varying the fraction of the atomizer output mixed into the humidified bulk N₂ flow. This approach allowed for the surface area concentration to be varied over the range of $3 \times 10^{-4} - 6 \times 10^{-3} \text{ cm}^2 \text{ cm}^{-3}$.

Depending on the aerosol number density needed for the kinetics experiments, one of two different CPCs (TSI 3010 and TSI 3025A) was employed to determine the particle number in each size bin of a DMA scan. The majority of experiments utilized the TSI 3010 CPC, which can accurately count 10^4 particles cm^{-3} with $< 7\%$ coincidence counting. A standard correction for coincidence counting was applied at all times. Typically, when atomizing a 1 wt% solution of malonic acid the maximum particle concentration observed in a size bin ranged from $< 10^4$ to about 4×10^4 particles cm^{-3} . The aerosol size range over which the maximum particle concentrations occurred generally accounted for $< 10\%$ of the total aerosol surface area. Therefore, uncertainties due to coincidence counting in this small number of bins are not expected to affect the accuracy of the total surface area, which we take to be $\pm 10\%$. However, when atomizing the more dilute solutions (0.1 and 0.3 wt% malonic acid), significantly higher particle number densities were required to produce surface area concentrations in the same range. In these cases, a TSI 3025A CPC, which can count 10^5 particles cm^{-3} without significant coincidence errors, was used.

A further set of experiments was performed using particles composed of azaleic acid. Given its trace solubility in water, azaleic acid particles were generated by homogeneous nucleation using ~ 1 g of azaleic acid packed into the lower half of a 1.3 cm OD pyrex tube. The pyrex tube was 30.5 cm long, half of the length, where the

azaleic acid was present, was wrapped in heating tape and covered with insulation while the other half was exposed. The pyrex tube was heated to ~ 370 K and a small flow (100-300 sccm) of dry N₂ passed through the tube. At this temperature, there was enough azaleic acid in the vapor to homogeneously nucleate particles. The small flow through the homogeneous nucleation source was mixed into a humidified bulk N₂ flow of 3-4 slpm. For these experiments, the RH was measured with the in-line hygrometer probe, and because azaleic acid particles are not likely to deliquesce until $\sim 100\%$ RH, the phase determination region was bypassed. In contrast to the atomizer output, the homogeneous nucleation source provides a narrow size distribution with $\sigma_{\text{gm}} = 1.25$ and a typical number weighted $d_{\text{gm}} = 130$ nm which depends on the temperature and flow rate through the source. Total surface area concentration was changed during an experiment by changing the temperature (to affect a size change) and/or by mixing a larger flow from the homogeneous nucleation source into the humidified bulk flow.

2.2 N₂O₅ Synthesis and Delivery

N₂O₅ was synthesized in a 50 cm long, 2 cm OD, pyrex flow tube by mixing a small flow of pure NO₂ in a larger flow of O₂ (~ 0.5 slpm) containing excess O₃ (to oxidize NO₂ to NO₃) generated by passing the O₂ flow along a Hg lamp (Jelight Co.). Prior to synthesis, the reaction manifold was purged with dry N₂ for several minutes, and the O₂ used to generate O₃ was passed through a Drierite trap. N₂O₅ produced from the reaction of NO₃ with NO₂ was trapped as a white solid in a pyrex flask held at 190 K (ethanol slush bath). N₂O₅ was stored for weeks at a time at ~ 220 K by use of a cold finger (Neslab C60).

To control the amount of N₂O₅ delivered to the kinetics flow tube, the N₂O₅ trap was kept at ~ 208 K for the majority of data presented here. An extrapolation of *Stull's* data^{20,21} suggests a vapor pressure of ~ 0.006 Torr for N₂O₅ at 208 K. This extrapolation is consistent with N₂O₅ vapor pressure estimates for similar temperatures by *Hanson and Ravishankara*.²² A small flow of N₂ (1-5 sccm) was sent through the trap and we assume from previous work¹⁶ that this flow became saturated in N₂O₅ vapor. Flow eluting from the trap was immediately mixed into a larger N₂ flow of 95-99 sccm for a total flow of 100 sccm containing ~ $6 \times 10^{-5} - 3 \times 10^{-4}$ Torr N₂O₅. This mixture was transported through ~ 3 m of 3 mm OD PFA Teflon tubing (residence time ~ 13 s) to the kinetics flow reactor. We estimate an absolute accuracy of $\pm 50\%$ for the N₂O₅ partial pressures.

2.3 Entrained Aerosol Flow Reactor

The central portion of the experimental setup consisted of a 90 cm long vertically oriented pyrex flow tube with a 3 cm ID. This flow reactor was coupled to a custom-built chemical ionization mass spectrometer for the detection of N₂O₅. A schematic of this portion of the setup is shown in Figure 3. A rotary vane pump was used to draw a portion of the humidified aerosol flow into the top of the flow reactor through a perpendicular side-arm. Excess flow was directed into the house exhaust system. The flow tube was maintained at atmospheric pressure and room temperature (avg. 755 Torr and 300 K). The volumetric flow rate through the reactor was regulated to be constant during an experiment by a pinhole in a stainless steel disc contained within a Cajon UltraTorr fitting and located at the bottom end of the flow tube. The volumetric flow rate through the pinhole was routinely calibrated prior to or after an experiment by measuring the

pressure on the low-pressure side of the pinhole as function of flow rate through an MKS flowmeter. In most experiments, the volumetric flow rate was 1.45 slpm but ranged from 1.25-1.5 slpm in a few experiments using different sized pinholes. These flow characteristics led to a linear flow velocity of about 4 cm s⁻¹ and a Reynolds number of ~ 120 implying laminar flow conditions down the majority of the flow tube length. The entrance length required for the full development of laminar flow under these conditions is ~ 15 cm from the point of introduction of the humidified aerosol flow.²³ Over the course of a kinetics experiment a small amount of aerosol was observed to build up on the walls of the upper end of the flow reactor near the 90° bend at the point of introduction. Measurements of aerosol surface area taken at the top and the bottom of the flow tube agreed to within 10% and thus we assume this slow buildup constituted a negligible loss of aerosol surface area in the flow reactor during a kinetics run.

A moveable 6 mm OD pyrex tube was inserted axially down the center of the flow tube serving to inject the 100 sccm flow of N₂O₅ in N₂ into the central portion of the humidified aerosol flow. N₂O₅ concentrations in the flow tube ranged from ~ 1.5x10¹¹ – 7x10¹¹ molec cm⁻³ (6-30 ppbv/ 1 atm). For experiments performed with solid malonic and azaleic acid aerosol, a higher initial N₂O₅ concentration of ~ 5x10¹² molec cm⁻³ was used. For a gas-phase diffusion constant of ~ 0.1 cm² s⁻¹,¹⁶ the characteristic time for N₂O₅ to fully mix into the aerosol flow is estimated to be ~ 4.5 s,²⁴ corresponding to about 18 cm down the length of the flow tube. To ensure kinetics were obtained under fully developed laminar flow and with N₂O₅ fully mixed into the bulk aerosol flow, decays of N₂O₅ as a function of injector distance were performed by starting 25 cm above the bottom of the flow tube and ending ~ 25 cm below the introduction of the bulk flow. In the majority of

experiments, the interior walls of the flow tube were coated with a thin layer of halocarbon wax to minimize N₂O₅ wall loss, and the flow tube was washed and dried between most experiments.

2.4 N₂O₅ Detection

N₂O₅ was detected as NO₃⁻ by chemical ionization mass spectrometry (CIMS) using I⁻ as a reagent ion via: $I^- + N_2O_5 \rightarrow NO_3^- + INO_2$. This detection scheme has been used to selectively detect N₂O₅ in the presence of HNO₃,²⁵ and its implementation is similar to that by *Hu and Abbatt*¹⁶. In the CIMS source region, I⁻ reagent ions were produced by flowing 2.8 slpm of N₂, carrying trace amounts of CH₃I (Aldrich), over a radioactive ²¹⁰Po source (NRD Inc. P-2021 inline ionizer). The ²¹⁰Po ion source was fixed to the end of a 6 mm OD stainless steel tube which ran perpendicular to the aerosol flow reactor down the axis of a 2.54 cm OD pyrex tube. A stainless steel 2.3 cm ID sheath was inserted snugly into the pyrex tube. The ion source and this sheath were biased from –100 to –150 V to aid in the transmission of ions to the mass spectrometer aperture which was biased to –80 V. The mouth of the ion source was approximately 2-3 cm from the front aperture of the mass spectrometer housing. An additional 5.8 slpm of N₂ passed around the ion source for a total 7-fold dilution of the flow from the aerosol kinetics tube.

N₂O₅ reacted with the I⁻ reagent ions in the short distance between the ion source and the mass spectrometer entrance (~ 10 – 15 ms). Ions produced in the CIMS source region passed through 3 more stages of differential pumping to the quadrupole and Channeltron particle multiplier (Extrel). The first stage, at 1 Torr, acted as a declustering region to break apart weakly bound ion-H₂O clusters which can add complexity to

interpreting the mass spectra. Two ion lenses inside the declustering region were biased to -75 V to aid in transmission through the region. The second stage of pumping was performed by a 500 L/s turbomolecular pump (Balzers). A pinhole biased to -30 V separated the declustering region from this second stage and dropped the pressure to $\sim 10^{-4}$ Torr. A slightly larger aperture in a skimmer cone biased to $+5$ V served as the entrance to the final stage of pumping performed with a 300 L/s turbomolecular pump (Varian). An Einzel lens stack directly behind this last aperture helped guide the ions into the quadrupole where they were mass selected and then detected with a Channeltron particle multiplier operated in single negative ion counting mode.

Under dry conditions (RH < 10%), this detection scheme provided a signal count rate of ~ 3000 Hz for 30 ppbv N₂O₅ in the aerosol flow reactor when the reactor output was mixed directly in front of the radioactive ion source. This analyte signal was generally < 1% of the reagent ion signal ($> 3 \times 10^5$ Hz). Under humidified conditions, the sensitivity to N₂O₅ in the flow reactor degraded by nearly a factor of 2 at 50% RH most likely due to the loss of N₂O₅ on surfaces between the reactor and the CIMS source region. The presence of aerosol particles in the flow, or a buildup on the walls, would degrade the sensitivity further reaching signal rates of ~ 800 -900 Hz for 30 ppbv N₂O₅ in the aerosol flow tube under these conditions. Background count rates were typically < 10 Hz at the NO₃⁻ mass. Therefore, under the degraded signal conditions of a typical high RH experiment (signal rate of 900 Hz/ppbv), this scheme provided a 1-Hz detection limit (S/N = 1) of ~ 150 pptv N₂O₅ in the flow reactor, corresponding to $\sim 4 \times 10^9$ molec cm⁻³ at atmospheric pressure. Given the 7-fold dilution that occurs, this implies a 1-Hz detection

limit of $\sim 1.2 \times 10^8$ molec cm⁻³ in the CIMS source region. Efforts are in progress to avoid this dilution by maintaining the CIMS source region at atmospheric pressure.

The CIMS scheme provided a clean mass spectrum. We note that a signal at 190 amu attributed to a I•HNO₃⁻ cluster was observed but did not respond reproducibly to changes in N₂O₅ concentrations. Under conditions of long ion-molecule reaction times a significant background signal at the NO₃⁻ mass was observed when N₂O₅ had been completely reacted away. This signal was highly non-linear with ion-molecule reaction time but, when observed, was typically 10% of the initial N₂O₅ signal. This background was attributed to HNO₃ either reacting directly with I⁻ to form HI and NO₃⁻ as products, or from a large fraction of the observed I•HNO₃⁻ cluster falling apart to yield NO₃⁻. All of the results reported here were obtained at short ion-molecule reaction times where this chemical background was indistinguishable from random noise. However, we note that for long ion-molecule reaction times, subtracting off the observed chemical background from the decay data yielded the same first order rate constants as those taken with short ion-molecule reaction times and all other experimental conditions the same. A non-negligible signal at 103 amu attributed to the malonate ion (HOOCHCH₂CHOO⁻) was also observed. Its intensity was strongly determined by the magnitude of NO₃⁻, and could be minimized to be < 25% of the NO₃⁻ signal by increasing the electric field between the ion source and the front aperture of the mass spectrometer housing, suggesting a secondary ion process. We believe the reaction between NO₃⁻ and gas phase malonic acid, from the impaction of malonic acid aerosol in the CIMS region, resulted in the malonate ion and HNO₃. Because NO₃⁻ is a strong gas-phase base,²⁶ it is likely that this was a non-equilibrium reaction, not affecting the linearity of response to N₂O₅.

3. Results

Figure 4 shows a plot of N₂O₅ decays obtained with different average total surface area concentrations, S_a (cm² per cm³ of air), of aqueous malonic acid aerosol present at 50% RH. Mean N₂O₅ signal (Hz) is plotted on a log-scale versus injector distance. Error bars represent the 1σ variation of N₂O₅ signal used in calculating the mean at each distance. This variation was used in generating uncertainty-weighted least squares linear fits to the natural log of the N₂O₅ signal versus distance. Within the error of the data, the decays were well described by first-order kinetics. Note that there is a small loss of N₂O₅ in the absence of aerosol particles. These “wall” decays were performed after each aerosol decay, or interpolated between at most two sequential aerosol decays. Distances shown in Figure 4 were converted to reaction times using the bulk flow velocity and resulting first-order rate constants were corrected for non-plug flow conditions via a standard iterative method described by *Brown*.²⁷ Inputs into this routine were, i) the observed N₂O₅ wall loss rate, which typically ranged from less than 0.003 s⁻¹ increasing slightly with RH for a halocarbon wax coated tube to ~ 0.01 s⁻¹ for an uncoated tube, ii) the overall observed N₂O₅ decay rate in the presence of aerosol particles, iii) the gas-phase diffusion constant for N₂O₅ 0.1 cm²/s, and iv) the bulk flow velocity in the aerosol flow reactor. The corrected first order rate constants, k¹_{obs}, due solely to loss on aerosol, were typically 10-25% higher than their observed inputs.

Figure 5 shows the corrected first-order rate constants, obtained from the decays in Figure 4, plotted versus the average S_a measured during the given decay. Additional rate constants determined from the same experiment are also included. The error bars in

Figure 5 are the estimated random uncertainty in the rate constants as determined from the calculated uncertainty in the slopes of the weighted least squares fit to the decay data shown in Figure 4. We assume this uncertainty (typically 5-10%) captures the bulk of the random errors in the first order decays. Variability in S_a measured during a decay, typically $\pm 5\%$ (1σ), is an additional source of scatter.

The first-order rate constants are related to gas-particle uptake coefficients, to a first approximation, by Equation 1:

$$k_{\text{obs}}^{\text{I}} = \frac{\gamma v}{4} S_a \quad (1)$$

where γ is the uptake coefficient, and v is the mean molecular speed of N₂O₅. Equation 1 neglects the effects of gas-phase diffusion limitations which can be corrected for as described by *Fuchs and Sutugin*.²⁸ We have estimated that this correction is negligible (< 3.5%) for the aerosol size range and relatively small reaction probabilities we have observed. Therefore, we report uptake coefficients derived from equation 1. Uptake coefficients are calculated from the slope of a weighted linear least squares fit to a plot of $k_{\text{obs}}^{\text{I}}$ versus measured total surface area concentrations (e.g., Figure 5) obtained for a given RH. Forcing the fit to pass through the origin generally brings the uptake coefficient calculated from the slope into agreement with the mean uptake coefficient calculated from individual $k_{\text{obs}}^{\text{I}}$ and S_a using equation 1. We note, however, that it is important to demonstrate a linear relationship as per equation 1 for confidence that significant systematic biases in the observed kinetics do not exist.

Measured uptake coefficients, γ_m , for the hydrolysis of N₂O₅ on malonic acid and azelaic aerosol are plotted both as a function of RH (top panel) and aerosol liquid water

content (bottom panel) in Figure 6. Results on aqueous malonic acid results are also summarized in Table 1. The error bars in Figure 6 represent the 1σ deviation of data about the mean. Three features are evident in the top panel of Figure 6. First, we were unable to measure an N₂O₅ decay rate that was statistically different from our wall-loss on solid malonic acid aerosol over the RH range from 0-50%. For these experiments, the flow reactor walls were not coated with halocarbon wax leading to a higher wall loss. Nonetheless, we report a conservative upper limit for the uptake coefficient under these conditions, i.e., $\gamma_m < 0.001$ (asterisks). Second, adding support to this value are the measurements performed on solid azaleic aerosol at 85% RH (open star) with the wall-loss having been reduced by an order of magnitude by a coating of halocarbon wax. The first-order rate constants due to N₂O₅ loss on azaleic aerosol, while being statistically different from the wall loss, did not appear strongly correlated to changes in aerosol surface area concentrations. We therefore set an upper limit to the uptake coefficient to be $5 \pm 3 \times 10^{-4}$. Third, γ_m on aqueous malonic acid aerosol (triangles and open circles) exhibit a strong dependence on RH, and a moderate inverse dependence on initial N₂O₅ concentration. For example, γ_m for aqueous malonic acid aerosol determined with 30 ppbv N₂O₅ (triangles) increase from 0.002 at 10% RH up to 0.025 at 50% RH. Above 50% RH, γ_m appears to be constant at ~ 0.025 to within the 1σ variation of the measurements. As a guide towards a possible mechanism for the observed dependence of γ_m on RH for aqueous malonic acid aerosol, we show these same γ_m plotted versus the aerosol liquid water molarity estimated from data by *Braban et al.*¹⁰ and *Peng et al.*¹¹ The γ_m obtained for RH < 50% exhibit a strong linear correlation ($r^2 = 0.99$) with aerosol liquid water concentration, [H₂O]_a. For example, the slope of a least-squares linear fit

(not shown) to data obtained with 30 ppbv N₂O₅, weighted by their uncertainty and forced through the origin, is $1.5 \times 10^{-3} \text{ M}^{-1}$. The 6 ppbv N₂O₅ data have the same slope, but a non-negligible intercept of 4×10^{-3} . The γ_m determined with 6 ppbv N₂O₅ initially in the flow tube are higher than those determined with 30 ppbv N₂O₅, and the effect is largest at lower RH (see Figure 7).

To further elucidate the cause for the observed dependence of γ_m on both RH ($[\text{H}_2\text{O}]_a$) and initial N₂O₅ concentration, we performed a set of kinetics experiments examining the dependence of γ_m on average aerosol size. These results are summarized in Figure 8 and Table 1. As discussed in the experimental section, atomizing 0.1, 0.3, and 0.1 wt% malonic acid solutions and subjecting the aerosol to 50% RH produced the size distributions shown in Figure 2. The geometric mean surface area-weighted particle radii for these distributions are 96, 107, and 143 nm, respectively, and in Figure 8, the associated γ_m are shown as squares. An additional set of experiments were performed by atomizing a 10 wt% malonic acid solution that yielded a geometric mean surface-weighted radius of 176 nm and the associated γ_m is shown as an asterisk. With respect to this latter point, while several determinations (> 15) of γ_m for this distribution lead to significantly higher precision, we note that we are less confident in its absolute accuracy.

A plot of $\frac{dS}{d \log D_p}$ versus $\log D_p$ for this size distribution suggested that we were unable to account for as much as 30% of the total surface area due to the DMA's inability to size particles larger than 1000 nm in diameter. The value for γ_m that we report, therefore, has been reduced by a factor 1.3 to account for this discrepancy, and the error bars increased to $\pm 25\%$. Most notably evident in Figure 8 is that for the smallest size aerosol particles

used, γ_m is lower than those determined on larger particles ($\gamma_m = 0.018 \pm 0.002$ c.f. $\gamma_m \geq 0.025$).

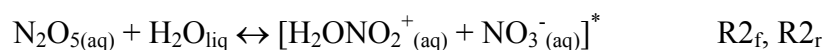
4. Discussion

There are few other published reports of reactive uptake coefficients for N₂O₅ hydrolysis in the presence of sub-micron organic aerosol over a large range in RH. It has been shown that a solid-like organic film (~ 15 nm thick) on sub-micron sulfate aerosol from the oxidation of alpha-pinene greatly reduced the uptake coefficient for N₂O₅.²⁹ Our results for uptake on solid malonic ($\gamma_m < 0.001$) and azaleic ($\gamma_m \sim 0.0005$) acid aerosol are consistent with these findings, as well as those for uptake onto other solid inorganic salts at moderate to low RH.¹⁴⁻¹⁸ The γ_m we observe on aqueous malonic acid aerosol (0.002 – 0.03) from 10 to 70% RH are well within the range of values reported for aqueous neutral inorganic aerosol.^{14-18,29,30} In fact, in most of these studies, γ_m approaches the value of ~ 0.025 at high RH. The systematic study of the effect of aerosol phase (i.e. composition) for organic aerosol that we report, together with similar studies on inorganic aerosols (e.g. (NH₄)₂SO₄, (NH₄)HSO₄)^{18,30} provide new insights into the mechanism of N₂O₅ hydrolysis. All of these studies provide evidence for a strong dependence on available H₂O at RH < 50%.

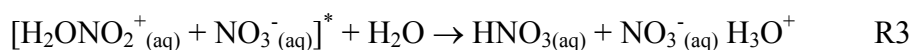
Whether N₂O₅ hydrolysis occurs in a thin layer near the aerosol surface or whether the reaction occurs throughout the aerosol volume continues to be an open question. In the analysis that follows, our goal is to determine whether our data supports one of these two extremes. We begin by assuming that the rate of N₂O₅ hydrolysis is limited by aerosol volume, and derive estimates of the first-order liquid phase rate

constant and the average depth an N₂O₅ molecule penetrates into the aerosol volume before reacting. We then compare these estimates to those derived from a detailed consideration of the observed size dependence. We conclude, in a summary below, that our results, while perhaps the most comprehensive in this regard to date, do not exclusively support either a volume-limited or surface reaction.

Our mechanism to explain N₂O₅ hydrolysis studies begins with accommodation of N₂O₅ into an aqueous surface layer followed by the formation of a hydrated intermediate:



In dilute acidic or neutral non-halide aerosol, further reaction of the intermediate with H₂O yields HNO₃ and dissolved nitrate via R3:



Depending on the pH, the HNO_{3(aq)} product of R3 will either dissolve to yield another NO₃⁻ or evaporate from the particle. The NO₃⁻ product of R3 can also form HNO₃ at low pH. It is important to note that reactions R2-R3, motivated by recent theoretical calculations,³¹ are meant to suggest that a concerted reaction between several water molecules and N₂O₅ to yield solvated HNO₃ is more likely to occur in neutral aqueous or moderately acidic solutions than is the solvation of N₂O₅ followed by auto-ionization to yield NO₂⁺ and NO₃⁻ as suggested by several authors.^{18,29,32,33} The product of R2_f represents a transient occurring along the concerted reaction pathway that is not likely to be an identifiable intermediate.³¹ This mechanism, without invoking NO₂⁺, explains observations that uptake is inhibited by NO₃⁻,^{15,18} and that halogen nitrites, such as ClNO₂, are products of N₂O₅ hydrolysis in aqueous sodium halide aerosol.^{17,32} The latter point implies that Cl⁻ reacts with the intermediate in R2_f more rapidly than H₂O. The

mechanism presented above (R2-R4) also explains a linear dependence on liquid H₂O concentrations observed by *Hallquist et al.*¹⁸ on neutral sulfate aerosol and in the data we present here.

Reactions R2 and R3 are also in line with the mechanism proposed by *Robinson et al.*³⁴ who argue that on highly acidic surfaces such as H₂SO₄ aerosol, an additional acid-catalyzed channel to yield NO₂⁺ as an intermediate is possible, but that at low H⁺_(aq) concentrations, such a channel is unlikely. They suggest under these conditions a direct hydrolysis reaction (R1) becomes the dominant channel. It is important to distinguish between N₂O₅ hydrolysis studies on H₂SO₄ surfaces and those on weakly acidic (such as those presented here) or neutral surfaces. Uptake coefficients for R1 on H₂SO₄ are on average higher, $\gamma_m \sim 0.03-0.1$,^{14,16,34-37} than those for more neutral surfaces, and show a very different RH dependence by decreasing with increasing RH.^{16,36}

The uptake coefficient is the convolution of mass accommodation to the surface, reaction at the surface, and solvation, diffusion, and reaction throughout the bulk. Within the framework of the resistor model,³⁸ which treats each of these processes as uncoupled, the uptake coefficient can be approximated as:

$$\frac{1}{\gamma} = \frac{1}{\Gamma_A} + \frac{1}{\Gamma_S + \Gamma_B} \quad (2)$$

where Γ_A , Γ_S , and Γ_B are the gas-phase collision frequency normalized rates for accommodation, surface-specific reaction, and bulk processes, respectively. Equation 2 neglects gas-phase diffusion constraints, which is reasonable for small particles (< 500 nm) and uptake coefficients < 0.05. A first-order rate constant for the loss of a gas-phase species is then given by equation 1. Because the reactivity of N₂O₅ in aqueous solutions is rapid, physico-chemical parameters, such as its solubility and liquid phase diffusion

constant, are undetermined. This lack of knowledge has precluded confirmation as to whether reaction R1 on aerosol characteristic of the troposphere is a surface-specific reaction, or whether N₂O₅ reaches saturation throughout the aerosol, with the reaction rate then limited by the available aerosol volume. A combination of these two extremes is also possible. The classification of R1 into one of these two extremes will have significant implications for how this reaction is treated in current global tropospheric chemistry models now incorporating distributions of aerosol of various compositions and phase.³⁹

4.1 Volume Dependent Mechanism

In order to determine whether the data we report here supports classification into either of these categories we begin by assuming that $\Gamma_S \ll \Gamma_B$ such that the concentration of N₂O₅ at the surface is in equilibrium with that just inside the surface. Under these conditions, the overall uptake coefficient for reaction on aerosol becomes:

$$\frac{1}{\gamma} = \frac{1}{\alpha} + \frac{v}{4HRT\sqrt{k^1D_1}} \left[\frac{1}{\coth(q) - \frac{1}{q}} \right] \quad (3)$$

where α is the mass accommodation coefficient, H is the Henry's law coefficient, R is the gas constant (moles L⁻¹ atm⁻¹ K⁻¹), T is the temperature (K), and q is a parameter which accounts for the competition between reaction and diffusion in a particle of finite size.³⁸

This competition is defined as

$$q = \frac{\ell}{r_p} \quad (4)$$

where r_p is the radius of the particle, and ℓ , the reacto-diffusive length, is given by

$$\ell = \sqrt{\frac{D_1}{k^I}} \quad (5)$$

This length is a proxy for the distance a molecule will diffuse before reacting, and therefore a measure of the concentration gradient of the reactant in the aerosol. In the case where $q > 1$, the particle becomes saturated with the gas-phase species, the reaction occurs throughout the volume of the particle, and equation 3 becomes equivalent to that for a volume-limited process, i.e.,

$$\frac{1}{\gamma} = \frac{1}{\alpha} + \frac{v}{4\text{HRT}k^I} \frac{S_a}{V_a} \quad (6)$$

where S_a/V_a is the ratio of the aerosol surface area and volume concentrations.

The near linear dependence of our measured uptake coefficients with the aerosol water concentration for relative humidities less than 50% strongly suggests that the rate of N₂O₅ loss under these conditions is limited by the liquid water volume. That is, if α is large (~ 1) compared to Γ_b

$$\frac{d[\text{N}_2\text{O}_5]}{dt} = -k^{II}[\text{H}_2\text{O}]_a V_a \text{HRT}[\text{N}_2\text{O}_5] \quad (7)$$

where k^{II} is the second-order rate coefficient for the reaction between N₂O₅ and water, and $k^{II}[\text{H}_2\text{O}]_a = k^I$ of equation 6. Under these assumptions ($q > 1$, $\alpha \gg \Gamma_b \gg \Gamma_s$) a plot of γ_m for $\text{RH} < 50\%$ versus the quantity $[\text{H}_2\text{O}]_a V_a/S_a$ should yield a straight line, the slope of which is $k^{II} \left(\frac{4\text{HRT}}{v} \right)$. This plot is shown in Figure 9. We have included all γ_m for

aqueous malonic acid aerosol with 30 ppbv N₂O₅ in the flow reactor (see Figures 6 and 7) separated into two categories: $\text{RH} < 50\%$ (solid circles) and $\text{RH} \geq 50\%$ (open squares).

The uncertainty-weighted least-squares linear fit shown in Figure 9 was restricted to only

those data for which RH < 50%. The Henry's law coefficient for N₂O₅ in these solutions is not known, so for the estimation of k^{II}, we assume H = 2 M atm⁻¹ which has been recommended for N₂O₅ in aqueous solutions of atmospheric nature.^{9,34} We derive a second-order rate constant for N₂O₅ hydrolysis, k^{II}, to be ~ 2.6x10⁴ M⁻¹ s⁻¹ for a temperature of 300 K. The product of k^{II} and the [H₂O]_a at 50% RH (17 M) yields a pseudo-first order rate constant, k^I, of 4.4x10⁵ s⁻¹ which is similar in magnitude to that estimated by *Folkers et al.* to be 2.5x10⁵ s⁻¹ for the rate limiting step in their proposed mechanism. Using our value k^I for 50% RH and an estimate of D₁ ~ 1x10⁻⁵ cm²/s,^{9,34} we can calculate the reacto-diffusive length from equation 5. This approach yields $\ell \sim 48$ nm, at 50% RH.

The observed size dependence of γ_m at 50% RH shown in Figure 8 provides a second, independent piece of evidence supporting a volume limitation to reaction R1 on super-saturated aqueous organic aerosol. If we continue to assume that $\alpha \gg \Gamma_b$, equation 3 simplifies to

$$\gamma = \gamma_{\text{thick}} \left[\coth(q) - \frac{1}{q} \right] \quad (8)$$

where γ is the uptake coefficient appropriate for small particles and γ_{thick}

$$\gamma_{\text{thick}} \approx \frac{4HRT\sqrt{k^I D_1}}{v} \quad (9)$$

is the uptake coefficient on very large particles (or thick films) where the time for diffusion out of the particle is long compared to that for reaction. Using our size dependence measurements as a guide, and assuming that $\gamma_{\text{thick}} \sim 0.03$ for malonic acid solutions at 50% RH, we estimate that $q = 0.6$ for particles with a surface-area weighted geometric mean radius of 95 nm. This result implies a $\ell \sim 40$ nm (see equation 4). This

value is essentially the same as that calculated above in an independent manner using equation 5 (48 nm). It is also worth noting that, to within 2σ of our measurement uncertainty (error bars shown in Figure 9 are 1σ), much of the data shown in Figure 9 can be explained by a $k^{\text{II}} \sim 2.6 \times 10^4 \text{ M}^{-1} \text{ s}^{-1}$. Deviations from this model for the 50% RH data are not completely understood, but not necessarily unexpected. For example, some deviation is likely due to the reacto-diffusive length decreasing rapidly with increasing RH, possibly leading to γ_m being in a non-linear transition region away from a volume dependence. That is, we may be observing the transition from a volume-limited reaction to one occurring in a thin surface layer. Another is that aerosol composition is changing dramatically as the RH approaches and exceeds 70%, and assumptions about H , D_l , α , and for that matter, k^{II} , being constant for all relative humidities may not hold.

An inverse dependence of γ_m on the initial N₂O₅ concentration was observed on aqueous malonic acid aerosol at all relative humidities examined (see Figures 6 and 7). Following on the above discussion, the initial N₂O₅ dependence in γ_m can be explained by NO₃⁻_(aq) inhibiting the ionization of N₂O₅ (R2). Results from partitioning calculations suggest that the fraction of HNO₃, produced by 30 ppbv N₂O₅ via reaction R1, remaining in the aerosol ranges from ~ 0.05 at 10% RH to 0.55 at 40% RH where it remains constant to 70% RH. For 6 ppbv N₂O₅, the fraction of particulate HNO₃ ranges from 0.1 to 0.7 over the same RH range. In these calculations, an iterative procedure is used where the effective Henry's law coefficient, H^* , is calculated first assuming all of the N₂O₅ is converted to HNO₃. The fraction of HNO₃ that would dissolve in an aerosol volume and pH given by the DMA measurements and malonic acid phase studies, respectively, is calculated from this initial H^* . The particle pH is recalculated to account for this amount

of HNO₃, and the resulting decrease in pH reduces HNO₃ solubility and therefore H^* . The procedure is repeated until the calculated particulate HNO₃ concentration converges to a value that is constant to within 1×10^{-4} M. The resulting HNO₃ concentrations in the particle, [HNO₃]_a, are estimated to range from ~ 0.25 M to 0.35 M for 30 ppbv N₂O₅ initially in the flow tube, with the lowest concentration at the highest RH. But the [HNO₃]_a also depend strongly on the total aerosol volume concentration measured. For 6 ppbv N₂O₅, [HNO₃]_a are estimated to be 3 – 4 times less than those for 30 ppbv N₂O₅ with the relative difference being greatest at highest relative humidities. Even with this iterative procedure, and neglecting HNO₃ from our N₂O₅ source which we expect to be on the order of N₂O₅ or less, we believe these estimates of nitrate concentrations can be considered upper limits given that during a typical decay, N₂O₅ was not completely reacted away.

Based on the above calculations, the “nitrate effect” we observe is rather small. The largest effect we observed was at 20% RH, where the γ_m was at most a factor of 2 larger with an estimated factor of 3 less nitrate present. At higher relative humidities, the effect was even smaller, approximately a 25% increase for greater than a factor of 3 in estimated nitrate concentrations. This small effect is still consistent with measurements of N₂O₅ hydrolysis made on NaNO₃ aerosol^{15,18,33} where the size of the nitrate effect was inversely related to the RH. For example, *Wahner et al.*³³ report $\gamma_m \sim 0.002$ at 48% RH and $\gamma_m = 0.024$ at 88% RH. In these experiments the [NO₃⁻]_(aq) are at least an order of magnitude higher than those estimated here, even for the most dilute particles studied. Thus, a slight effect, even for a large relative change in nitrate concentration might be expected if the rate of reaction R3_r had become negligible compared to the forward

reaction. To our knowledge, our results are the first to show a dependence of the γ_m on the initial partial pressure of N₂O₅ for aqueous aerosol. Studies on solid sulphate salt particles¹⁸ and H₂SO₄ surfaces^{35,36} did not observe a dependence on N₂O₅ partial pressure, and similarly *Kane et al.*³⁰ report that an effect was not observed but the surface on which they tested this effect is unclear. We note, however, that the highest N₂O₅ concentrations typically used here (30 ppbv) are on the low end of, or much lower than, those used these other experiments.

From the above discussion, it is reasonable that for moderately acidic or neutral sub-micron aerosols, reaction R1 is a volume-limited process with $\alpha \gg \Gamma_b \gg \Gamma_s$ and that our data are consistent with the concerted ionization mechanism presented. This conclusion is similar to that made by *Hallquist et al.*¹⁸ but we note an important distinction. They suggest that because γ_m on aqueous sulfate aerosol reached a maximum at 50% RH and was constant to 70% RH in their experiments, this implied a mass accommodation limitation to a bulk process, and that $\alpha \sim 0.021$.¹⁸ We find that a similar, rigorous use of equation 2 requires α to be at least greater than 0.1 for a best fit to our observed γ_m . Also, an α of 0.021 would not be consistent with measurements made on larger (1-2 μm) (NH₄)₂SO₄ aerosol.¹⁶

4.2 Surface-Specific Reaction Mechanism

The complexity of this reaction system becomes apparent with a more in-depth view of the size dependence in conjunction with the estimated particulate [NO₃⁻_{(aq)]]. The observed size dependence leads to an initial conclusion that for 50% RH, ℓ is ~ 40 nm. However, the [NO₃⁻_{(aq)] that we estimate for the smallest particles used in the size}}

dependence study (50% RH) is greater than that estimated for larger particles at 20% RH where a non-negligible “nitrate effect” was observed. Thus, it is possible that the size dependence observed is at least partially a nitrate dependence. The agreement between the reacto-diffusive lengths calculated from the size dependence and an estimate of k^{II} is then a coincidence. This coincidence is not robust. For example, the estimated D_1 or H are probably not accurate to better than a factor of 2, and varying these within this range will affect the agreement between the calculated reacto-diffusive lengths. Furthermore, to within the precision of our size-dependent measurements, the choice of $\gamma_{\text{thick}} = 0.025$ (instead of 0.03) would be reasonable, leading to a $\ell \sim 26$ nm as opposed to 40 nm calculated above.

If the observed size dependence is complicated by a nitrate effect, the data presented here are also then consistent with N₂O₅ hydrolysis occurring at the surface or in a very thin layer near the surface. Surface-specific reactions may proceed via a Langmuir-Hinshelwood type mechanism.⁴⁰ The uptake coefficient due to reaction of N₂O₅ at the surface would therefore be linearly dependent with the surface concentration of H₂O^{40,41} and, depending on surface equilibria, may vary inversely with the initial gas-phase concentration of N₂O₅.⁴⁰ Clearly, our data on aqueous malonic acid aerosol show linearity with surface H₂O concentration, assuming a direct relationship between bulk and surface water concentration, and an inverse relationship with N₂O₅ concentration in the flow reactor. With respect to this latter point, the magnitude of this concentration dependence depends inherently on the number of surface sites and whether enough reactant molecules are present to saturate these sites. If N₂O₅ hydrolysis takes place at or near the surface, then to explain the large difference in uptake coefficients on solid and

aqueous organic aerosols, surface concentrations of H₂O, or available reactive sites, or N₂O₅ accommodation coefficients, on aqueous malonic acid aerosol would have to be factors of 10-100 higher than on solid malonic or azaleic acid aerosol at similar or even higher relative humidities.

5. Summary of Experimental Results

We report the first measurements of the uptake coefficient for N₂O₅ hydrolysis on organic aerosols. The measured uptake coefficients, γ_m , on aqueous malonic aerosol at RH > 50% are ~ 0.03 and suggest that the rate of N₂O₅ hydrolysis will not be suppressed relative to those on neutral inorganic aerosol by the inclusion of water-soluble organic material. However, γ_m are small (< 0.001) if the organic aerosols are solid. For relative humidity less than 50%, γ_m on aqueous malonic acid aerosol show a linear dependence on the aerosol liquid water content. These measurements are also the first demonstration of an N₂O₅ partial pressure dependence in the γ_m .

At this point, we cannot conclude that N₂O₅ hydrolysis is a volume-limited process or whether it occurs in a small surface layer. Our observations suggest that the reacto-diffusive length for R1 on super-saturated and dilute aqueous malonic acid aerosol may be ~ 50 nm to less than 25 nm at 50% RH. Future experiments performed on very small particles (surface area-weighted radius < 100 nm) or on aerosol particles containing a solid, un-reactive core, with an aqueous coating, the thickness of which is variable, may be able to resolve this issue. Additionally, these future experiments on sub-micron aerosol should be performed with N₂O₅ concentrations less than 1.5×10^{11} molec cm⁻³ (6 ppbv, 760 Torr) in order to avoid possible surface saturation and/or nitrate effects.

6. Atmospheric Implications

The heterogeneous hydrolysis of N₂O₅ has now been studied on a wide variety of substrates across a wide range of RH, temperature, and composition, including but not limited to, ice,²² H₂SO₄ films,⁴² droplets,³⁴ and aerosol particles,^{14,16,30,35-37} neutral sulfate aerosol,^{14,16,30} nitrate aerosol,^{15,18} sulfate aerosol with an organic coating,²⁹ and the organic aerosols presented here. While a single mechanism has yet to be proposed which universally explains the observed uptake coefficients on all surfaces,³⁴ general conclusions can be drawn about the appropriate uptake coefficient to incorporate into global tropospheric chemistry models. First, it is evident from the studies we present here, that the presence of water-soluble organic material (such as small organic diacids) will have little effect on the rate of N₂O₅ hydrolysis as compared to that on aqueous inorganic aerosol. Second, the amount of available water (either surface or volume) appears to most strongly control the rate of R1 on mildly acidic or neutral aqueous aerosols. It is important to note that even on highly super-saturated aqueous solutions we observe $\gamma_m \sim 0.015$, making R1 an important loss of NO_x on low nitrate aqueous aerosols at all relevant relative humidities. Third, it seems unlikely that there will be sufficient surface-water present on solid aerosol particles (hygroscopic or hydrophobic) to make R1 an important loss of NO_x on these types of particles at any RH. However, this latter conclusion needs to be verified for the range of atmospherically relevant N₂O₅ and particulate NO₃⁻ concentrations.

It is striking that on ice and sub-micron aqueous aerosol of all types at high RH, γ_m approaches 0.025-0.03, close to the recommended value for pure water at 292 K,

0.022.⁴³ Most global tropospheric chemistry models currently assume $\gamma = 0.1$ for reaction R1 on sulphate aerosol, likely based on experiments performed for H₂SO₄ surfaces under stratospheric conditions.^{38,39} As noted in the discussion, it is probably prudent to separate the treatment of N₂O₅ hydrolysis on highly acidic H₂SO₄ aerosol from that on more neutral aqueous aerosols. This is especially true for the troposphere where a large fraction of aerosols is nearly neutralized by NH₃, especially over continental regions.⁹ Based on our experiments, and those cited herein, we recommend that for a single uptake coefficient, $\gamma = 0.03 - 0.05$ is more appropriate for N₂O₅ hydrolysis on neutral aqueous aerosols in the troposphere. Incorporating a RH dependence to this γ is likely to be necessary, with $\gamma \sim 0.02$ at RH < 20% and reaching ~ 0.035 by 50% RH. The above recommendation is in concert with a recent modeling study by *Tie et al.*⁵ using measurements of NO_x and HNO₃ from the Arctic troposphere during winter finding that $\gamma \sim 0.06$ for N₂O₅ hydrolysis led to better measurement-model agreement.

The upper limit of our recommended γ is slightly larger than most experimental values to take into account the possibilities that experiments by our and other groups may have been compromised by high N₂O₅ concentrations leading to underestimated γ , and that a negative temperature dependence in the γ may exist. With respect to the latter point, a significant negative temperature dependence has not been observed on neutral aerosols,¹⁸ but we allow for the possibility given that there is evidence for one on highly acidic aerosol^{36,37} and pure water.⁴³

A systematic reduction in the N₂O₅ hydrolysis reaction probability in global tropospheric models will likely alter their predictions about the NO_x budget and the partitioning of NO_x among its reservoir species. Even with this reduction, reaction R1

will to continue to constitute an important nighttime loss of NO_x. For example, under high aerosol loading ($S_a \sim 1 \times 10^{-5} \text{ cm}^2 \text{ cm}^{-3}$) characteristic of a polluted region, N₂O₅ will have a lifetime with respect to heterogeneous loss of order 10 minutes if the uptake coefficient is 0.03. At temperatures less than $\sim 270 \text{ K}$, this is an order of magnitude shorter than that for thermal decomposition.

Acknowledgements

We acknowledge financial support from the National Science and Engineering Council (NSERC) of Canada and a Premiers Research Excellence Award (PREA Ontario) for J. P. D. Abbatt. The authors also thank Anthony Cox for sharing a pre-publication manuscript.

References

- 1 WMO. *Scientific Assessment of Ozone Depletion: 2002*, World Meteorological Organization, 2002, and references therein.
- 2 Dentener, F. J. and Crutzen, P. J. *J. Geophys. Res.-Atmos.* 1993, **98**, 7149-7163.
- 3 Tie, X., Brasseur, G., Emmons, L., Horowitz, L. and Kinnison, D. *J. Geophys. Res.-Atmos.* 2001, **106**, 22931-22964.
- 4 Brown, S. S., Stark, H., Ryerson, T. B., Williams, E. J., Nicks, D. K., Trainer, M. T., Fehsenfeld, F. C. and Ravishankara, A. R. *J. Geophys. Res.-Atmos.* 2003, **108**, 4299, doi:10.1029/2002JD002917.
- 5 Tie, X., Emmons, L., Horowitz, L., Brasseur, G., Ridley, B., Atlas, E., Stround, C., Hess, P., Klonecki, A., Madronich, S., Talbot, R. and Dibb, J. *J. Geophys. Res.-Atmos.* 2003, **108**, 8364, doi:10.1029/2001JD001508.
- 6 Geyer, A., Ackermann, R., Dubois, R., Lohrmann, B., Muller, T. and Platt, U. *Atmos. Environ.* 2001, **35**, 3619-3631.
- 7 Puxbaum, H., Novakov, T. and Hitzenberger, R. *Atmos. Environ.* 1999, **33**, 2601-2601.
- 8 Worsnop, D. R., Jayne, J. T., Canagaratna, M., Boudries, H., Kolb, C. E. and Jimenez, J. L. *Eos Transactions AGU* 2002, **83**, Fall Meeting Supplement, Abstract A11F-02.
- 9 Jacob, D. J. *Atmos. Environ.* 2000, **34**, 2131-2159, and references therein.
- 10 Braban, C. F., Styler, S. A., Carroll, M. F. and Abbatt, J. P. D. *J. Phys. Chem. A* 2003, **accepted**.

- 11 Peng, C., Chan, M. N. and Chan, C. K. *Environ. Sci. Technol.* 2001, **35**, 4495-4501.
- 12 Martin, S. T. *Chem. Rev.* 2000, **100**, 3403-3453, and references therein.
- 13 Hameri, K., Vakeva, M., Aalto, P. P., Kulmala, M., Swietlicki, E., Zhou, J., Seidl, W., Becker, E. and O'Dowd, C. D. *Tellus Ser. B-Chem. Phys. Meteorol.* 2001, **53**, 359-379.
- 14 Mozurkewich, M. and Calvert, J. G. *J. Geophys. Res.-Atmos.* 1988, **93**, 15889-15896.
- 15 Mentel, T. F., Sohn, M. and Wahner, A. *Phys. Chem. Chem. Phys.* 1999, **1**, 5451-5457.
- 16 Hu, J. H. and Abbatt, J. P. D. *J. Phys. Chem. A* 1997, **101**, 871-878, and references therein.
- 17 Schweitzer, F., Mirabel, P. and George, C. *J. Phys. Chem. A* 1998, **102**, 3942-3952.
- 18 Hallquist, M., Stewart, D. J., Stephenson, S. K. and Cox, R. A. *Phys. Chem. Chem. Phys.* 2003, **accepted**.
- 19 Kawamura, K., Kasukabe, H. and Barrie, L. A. *Atmos. Environ.* 1996, **30**, 1709-1722.
- 20 Stull, D. R. *Industrial and Engineering Chemistry* 1947, **39**, 517.
- 21 *CRC Handbook of Chemistry and Physics*; 71 ed.; Lide, D. R., Ed.; The Chemical Rubber Company, 1990.
- 22 Hanson, D. R. and Ravishankara, A. R. *J. Geophys. Res.-Atmos.* 1991, **96**, 5081-5090.

- 23 Kay, J. M. and Nedderman, R. M. *Fluid Mechanics and Transfer Processes*; Cambridge University Press: Cambridge, 1985.
- 24 Keyser, L. F. *J. Phys. Chem.* 1984, **88**, 4750-4758.
- 25 Huey, L. G., Hanson, D. R. and Howard, C. J. *J. Phys. Chem.* 1995, **99**, 5001-5008.
- 26 Davidson, J. A., Fehsenfeld, F. C. and Howard, C. J. *Int. J. Chem. Kinet.* 1977, **9**, 17-29.
- 27 Brown, R. L. *Journal of Research of the National Bureau of Standards* 1978, **83**, 1-8.
- 28 Fuchs, N. A. and Sutugin, A. G. *Highly Dispersed Aerosols*; Ann Arbor Science Publishers: Ann Arbor, 1970.
- 29 Folkers, M. and Mentel, T. F. *Geophys. Res. Lett.* 2003, **30**, 1644.
- 30 Kane, S. M., Caloz, F. and Leu, M. T. *J. Phys. Chem. A* 2001, **105**, 6465-6470.
- 31 McNamara, J. P. and Hillier, I. H. *J. Phys. Chem. A* 2000, **104**, 5307-5319.
- 32 Behnke, W., George, C., Scheer, V. and Zetzsch, C. J. *Geophys. Res.-Atmos.* 1997, **102**, 3795-3804.
- 33 Wahner, A., Mentel, T. F., Sohn, M. and Stier, J. J. *Geophys. Res.-Atmos.* 1998, **103**, 31103-31112.
- 34 Robinson, G. N., Worsnop, D. R., Jayne, J. T., Kolb, C. E. and Davidovits, P. J. *Geophys. Res.-Atmos.* 1997, **102**, 3583-3601.
- 35 Hanson, D. R. and Lovejoy, E. R. *Geophys. Res. Lett.* 1994, **21**, 2401-2404.
- 36 Hallquist, M., Stewart, D. J., Baker, J. and Cox, R. A. *J. Phys. Chem. A* 2000, **104**, 3984-3990.

- 37 Fried, A., Henry, B. E., Calvert, J. G. and Mozurkewich, M. *J. Geophys. Res.-Atmos.* 1994, **99**, 3517-3532.
- 38 Hanson, D. R., Ravishankara, A. R. and Solomon, S. *J. Geophys. Res.-Atmos.* 1994, **99**, 3615-3629.
- 39 Martin, R. V., Jacob, D. J., Yantosca, R. M., Chin, M. and Ginoux, P. *J. Geophys. Res.-Atmos.* 2003, **108**, 4097, doi:10.1029/2002JD002622.
- 40 Ammann, M., Poschl, U. and Rudich, Y. *Phys. Chem. Chem. Phys.* 2003, **5**, 351-356.
- 41 Hanson, D. R. *J. Phys. Chem. B* 1997, **101**, 4998-5001.
- 42 Hanson, D. R. *Geophys. Res. Lett.* 1997, **24**, 1087-1090.
- 43 Sander, S. P., Friedl, R. R., DeMore, W. B., Golden, D. M., Kurylo, R. F., Hampson, R. F., Huie, R. E., Moortgat, G. K., Ravishankara, A. R., Kolb, C. E. and Molina, M. J. *Chemical Kinetics and Photochemical Data for Use in Stratospheric Modeling, Evaluation Number 13*, NASA Jet Propulsion Laboratory, California Institute of Technology, 2000.

Figure and Table Captions

Table 1. Uptake Coefficients on Aqueous Malonic Acid Aerosol. All data for uptake coefficients measured on aqueous malonic acid aerosol is tabulated. RH is relative humidity, $sw-r_p$ is the geometric mean surface area-weighted aerosol radius, V_a is the mean aerosol volume, and V_a/S_a is the mean volume-to-surface ratio.

Figure 1: Schematic of the aerosol phase determination apparatus. See text for details.

Figure 2: Number-weighted (top panel) and surface area-weighted (bottom panel) size distributions of malonic acid aerosol generated from the atomizer. Three distributions are shown from atomizing 1 (circles), 0.3 (squares), and 0.1 (triangles) wt% solutions of malonic acid in water.

Figure 3: Schematic of the entrained aerosol flow tube and chemical ionization mass spectrometer. See text for details.

Figure 4: N₂O₅ signal (Hz) versus injector distance (cm) during kinetic runs where initial mixing ratio of N₂O₅ is 30 ppbv. Signal decay with no aerosol particles present (wall loss) is shown with circles. Three decays performed with three different surface area concentrations of aqueous malonic acid aerosol at 50% RH are shown with triangles (see legend). Lines represent 1 σ error-weighted least squares linear fits to the data.

Figure 5: Corrected first order rate constants, k_{obs}^1 (s⁻¹), for the decay of N₂O₅ in the presence of aqueous malonic acid aerosol at 50% RH are shown versus surface area concentration (cm² cm⁻³). The line represents a 1 σ error-weighted least squares fit forced through the origin.

Figure 6: Measured uptake coefficients, γ_m , are plotted versus RH (top panel) and estimated aerosol liquid water concentration, $[\text{H}_2\text{O}]_a$ (M) (bottom panel). In the top panel, asterisks are γ_m determined on solid malonic acid aerosol and the star is that on solid azelaic acid aerosol. Two sets of γ_m for aqueous malonic acid aerosol are shown, one set for those determined with 30 ppbv N₂O₅ (triangles), and one for those determined with 6 ppbv. In the lower panel, only the γ_m for aqueous malonic acid aerosol are shown.

Figure 7: The ratio of γ_m determined on aqueous malonic acid aerosol with 6 ppbv N₂O₅ to those determined with 30 ppbv is shown versus RH (bottom axis) and $[\text{H}_2\text{O}]_a$ (top axis).

Figure 8: Uptake coefficients determined on aqueous malonic acid aerosol at 50% RH are plotted versus the geometric mean of the surface area weighted particle radii. See text for details.

Figure 9: Measured uptake coefficients determined on aqueous malonic acid aerosol are shown versus the product of the aerosol liquid water concentration and the aerosol volume-to-surface ratio, $[\text{H}_2\text{O}]_a V_a/S_a$ (M nm). The solid circles are for RH < 50%, and the open squares are for RH ≥ 50%. The line represents a 1 σ error-weighted least squares linear fit to the circles (RH < 50%).

Table 1

RH %	sw-r _p nm	V _a 10 ¹³ nm ³ cm ⁻³	V _a /S _a nm	[H ₂ O] _a M	[N ₂ O ₅] 10 ¹¹ molec cm ⁻³	γ _m ± 1σ
10	170	1.1	68	2	7	0.002 ± 0.0005
20	169	1.6	70	4	1.5	0.011 ± 0.001
20	178	2.1	71	4	7	0.006 ± 0.0008
30	153	1.7	64	9	1.5	0.019 ± 0.002
30	187	2.3	74	9	7	0.014 ± 0.002
40	191	2.4	77	13	7	0.022 ± 0.0035
50	151	0.9	63	17	1.5	0.031 ± 0.003
50	143	1.2	60	17	7	0.025 ± 0.002
50	96	0.24	40	17	7	0.018 ± 0.003
50	107	0.6	44	17	7	0.025 ± 0.003
50	176	1.1	73	17	7	0.031 ± 0.008
70	154	1.0	65	27	1.5	0.033 ± 0.005
70	146	1.1	63	27	7	0.028 ± 0.003